

Pairing and charge distribution in Emery ladders preserving the ratio of Cu to O atoms

Gökmen Polat and Eric Jeckelmann

Leibniz Universität Hannover, Institute of Theoretical Physics, Appelstr. 2, 30167 Hanover, Germany

(Dated: March 12, 2026)

We study the Emery model (three-band Hubbard model) for superconducting cuprates on three distinct ladder-like lattices that are supercell of the CuO_2 plane and thus preserve the ratio of copper to oxygen atoms. Using the density-matrix renormalization group method we confirm that these Emery ladders are charge-transfer insulators for the hole concentration corresponding to undoped cuprates but become Luther-Emery liquids with enhanced pairing correlations upon doping. The preservation of the Cu to O ratio allows us to study the distribution of charges between these atoms in the Luther-Emery phase. We show that these Emery ladders can describe the relations between charge distribution, pairing strength, and interactions that have been observed in the Emery model on two-dimensional clusters and in experiments.

I. INTRODUCTION

Understanding cuprate high-temperature superconductors remains a theoretical challenge forty years after their discovery [1]. The two-dimensional (2D) Emery model (or three-band Hubbard model) [2] is generally believed to describe the low-energy electronic properties of these materials [3]. As this model includes both copper and oxygen orbitals of the CuO_2 planes, it allows one to describe undoped cuprates as charge-transfer insulators and to investigate the charge distribution between copper and oxygen atoms in doped cuprates [4–8]. Given the difficulty of studying 2D strongly correlated systems, quasi-one-dimensional (1D) subsystems called ladders have often been investigated with the aim of shedding light on the properties of their 2D parents [9, 10]. The advantage of ladder systems is the availability of well-established methods for 1D correlated models such as the density-matrix renormalization group (DMRG) [11–15]. The Emery model has been studied on two-leg ladders using the DMRG method for nearly 30 years [4, 16, 17]. Recently, this approach has been used [18–23] to investigate the existence of a Luther-Emery phase with enhanced pairing correlations [24], which is the 1D counterpart of the superconducting phase in higher dimensions.

In our previous work [23], we demonstrated the existence of a robust Luther-Emery phase with enhanced pairing correlations in the three common ladder structures used in other works [4, 16–22], which we called 3-chain ladder, 5-chain ladder, and 4-chain tube. However, the ratio of Cu to O orbitals is 2:3 and 2:5 in the 3-chain and 5-chain ladders, respectively, which differs significantly from the ratio 1:2 of the 2D CuO_2 lattice. The 4-chain tube has the right ratio but pairing occurs only if the hopping terms between Cu and O orbitals are anisotropic. Thus it is questionable whether these common ladders can approximate the essential properties of the isotropic 2D CuO_2 lattice, especially, the charge distribution between Cu and O atoms.

In this work we propose three two-leg ladder structures with a Cu to O ratio of 1:2. Each ladder can be

seen as a supercell of the 2D CuO_2 lattice. A drawback is that they have lower symmetries than the common ladder structures. We study the Emery model on the proposed ladder structures and show that they exhibit the low-energy properties expected for cuprates with realistic parameters. In particular, they are charge-transfer insulators for the hole concentration corresponding to undoped cuprates but become Luther-Emery liquids upon doping. This allows us to study the distribution of charges between copper and oxygen atoms as well as the pairing strength as a function of doping and Hamiltonian parameters. We find systematic relations in agreement with experimental results [25, 26] and theoretical predictions for 2D clusters [5–8].

The structure of the paper is as follows: In Sec. II, we introduce the ladder structures, the Emery model and the method used. We discuss the properties of the ladders at hole concentration corresponding to undoped cuprates in Sec. III. In Sec. IV we investigate their pairing properties upon electron and hole doping. The charge distribution on the oxygen and copper orbitals is discussed in Sec. V. Finally, we present our conclusion in Sec. VI.

II. MODEL AND METHOD

A. Ladder structures

The low-energy electronic excitations of superconducting cuprates are confined in their CuO_2 planes [3, 27]. Thus many efforts have been devoted to understanding the properties of strongly correlated electron systems on 2D lattices. However, most numerical approaches can only handle small subsystems of 2D lattices accurately. In particular, the DMRG method has been very successfully applied to ladder lattices. The original Hubbard ladders [28] are simply made of two coupled 1D Hubbard chains and they can be seen as narrow strips cut out of a square lattice.

For the 2D CuO_2 lattice, however, there are many possibilities of cutting out a strip of Cu and O atoms. Several

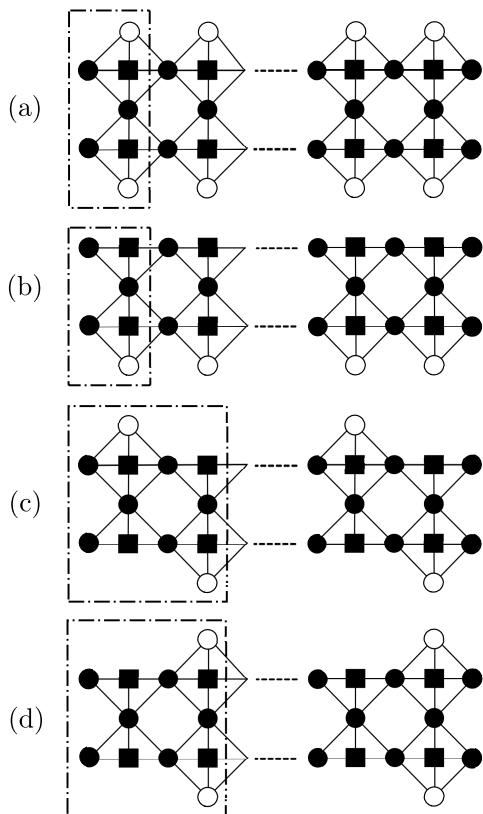


FIG. 1. Schematic of various two-leg ladder lattice structures. Squares and circles represent copper d orbitals and oxygen p orbitals, respectively. Solid black circles and squares are included in all lattice structures. White circles denote the outer oxygen p orbitals that are included in specific ladders only. Dashed-dotted lines indicate the unit cells. Solid lines represent the hopping terms between orbitals in the Emery model (1). (a) Three-chain ladder made of the solid black symbols, five-chain ladder made of all symbols, and four-chain tube, where the upper and lower white circles represent the same oxygen atoms, (b) t-ladder with translation symmetry, (c) g-ladder with glide symmetry, and (d) r-ladder with reflection symmetry.

ladder structures for cuprates are shown in Fig. 1. All examples in this figure are two-leg ladders composed of two chains of copper atoms and a variable number of oxygen atoms. Figure 1(a) illustrates three common ladder structures that have already been studied in the framework of the Emery model [4, 16–23]: the three-chain ladder, the five-chain ladder, and the four-chain tube. Note that they possess a reflection symmetry in the rung direction (vertical or y -direction) and that infinitely long ladders also have a discrete translational invariance in the leg direction (horizontal or x -direction).

Although the study of these ladders has yield much information about the properties of the Emery model, their adequacy for investigating the properties of 2D systems is questionable [23]. Indeed, these ladders cannot be seen as a supercell of the 2D CuO_2 lattice, i.e we do not recover the correct 2D lattice structure by repeating

Ladder	Unit cell	T_1	T_2	R
3-chain	Cu_2O_3	✓	✓	✓
5-chain	Cu_2O_5	✓	✓	✓
tube	Cu_2O_4	✓	✓	✓
t	Cu_2O_4	✓	✓	-
g	Cu_4O_8	-	✓	-
r	Cu_4O_8	-	✓	✓

TABLE I. Unit cell and symmetries of the six ladder structures illustrated in Fig. 1. T_1 indicates that an infinitely long ladder is invariant under discrete translations in the leg direction with a period equal to the lattice constant of the 2D CuO_2 lattice. T_2 corresponds to a twice longer lattice period. R indicates a reflection symmetry in the rung direction.

periodically one of these ladder structures. An obvious inconsistency is that the ratio of Cu to O atoms is 2:3 and 2:5 in the 3-chain and 5-chain ladders, respectively, instead of the ratio 1:2 in the 2D CuO_2 lattice. This is an important issue when studying the charge redistribution between Cu and O atoms as discussed in Sec. V. The four-chain tube has the correct ratio of both atoms but as a result of the periodic hopping terms in the rung direction, it exhibits a Luther-Emery phase only for hopping terms that are stronger in the leg direction than in the rung direction [23], which is not compatible with the symmetry of the 2D CuO_2 lattice under 90 degree rotations.

However, various two-leg ladder structures that are supercells and thus have the correct ratio of Cu to O atoms can be cut out of the 2D CuO_2 lattice. Three examples are shown in Fig. 1(b) to (d). Obviously, they possess a lower symmetry than the common ladders shown in Fig. 1(a). The t-ladder in Fig. 1(b) preserves the discrete translational invariance but breaks the reflection symmetry. The g-ladder in Fig. 1(c) possesses a glide symmetry instead of the separate translation and reflection symmetries. Thus its unit cell is twice as large as for the common ladder structures. Finally, the r-ladder in Fig. 1(d) preserves the reflection symmetry in the rung direction but its periodicity in the leg direction is also twice as long as for the common ladder structures. The symmetries and unit cells are summarized in Table I.

B. Hamiltonian

The Emery model [2, 3] extends the Hubbard model to describe holes in the pertinent orbitals of a 2D CuO_2 lattice. The model incorporates one $d_{x^2-y^2}$ orbital for each copper atom and one p_x or p_y orbital for each oxygen atom. We apply this model to the two-leg ladders shown in Fig. 1. The system size L is defined as the number of d orbitals on a single leg. This is also the number of rungs in the ladder. The undoped state corresponds to a filling of $N = 2L$ holes. The doping concentration is defined as $\delta = N/(2L) - 1$. Thus $\delta = 0$ corresponds to

an undoped ladder, $\delta > 0$ when the system is hole-doped but holes are removed ($\delta < 0$) upon electron doping.

The Hamiltonian is

$$\begin{aligned}
H = & - t_{dp_x} \sum_{\langle ij \rangle, \sigma} \left(p_{xi\sigma}^\dagger d_{j\sigma} + \text{H.c.} \right) \\
& - t_{dp_y} \sum_{\langle ij \rangle, \sigma} \left(p_{yi\sigma}^\dagger d_{j\sigma} + \text{H.c.} \right) \\
& - t_{pp} \sum_{\langle ij \rangle, \sigma} \left(p_{xi\sigma}^\dagger p_{yj\sigma} + \text{H.c.} \right) \quad (1) \\
& + \varepsilon \sum_{\alpha, i, \sigma} n_{\alpha i \sigma}^p \\
& + U_d \sum_i n_{i\uparrow}^d n_{i\downarrow}^d + U_p \sum_{\alpha, i} n_{\alpha i \uparrow}^p n_{\alpha i \downarrow}^p.
\end{aligned}$$

where $c_{i\sigma}$ is the annihilation operator and $c_{i\sigma}^\dagger$ is the creation operator for a hole with spin σ in a d orbital ($c = d$), a p_x orbital ($c = p_x$), or a p_y orbital ($c = p_y$). The hole number operators are defined by $n_{i\sigma}^d = d_{i\sigma}^\dagger d_{i\sigma}$ and $n_{\alpha i \sigma}^p = p_{\alpha i \sigma}^\dagger p_{\alpha i \sigma}$ with $\alpha = x, y$. The first three terms in the Hamiltonian represent hopping processes between neighbor orbital pairs. The first sum runs over all pairs $\langle ij \rangle$ made of nearest-neighbor d - p_x orbitals (represented by horizontal lines in Fig. 1) while the second sum is over all nearest-neighbor d - p_y pairs (vertical lines). The third sum runs over all nearest-neighbor p_x - p_y orbital pairs (represented by diagonal lines in Fig. 1). The fourth term in the Hamiltonian (1) is the energy difference between a single hole in a p orbital and one in a d orbital. The sum over the indices i and α indicates a sum over all p orbitals. The last two terms represent the Coulomb repulsion between two holes in the same d or p orbital, respectively, and their sums run over all corresponding orbitals.

The Hamiltonian (1) comprises six parameters. First, there are the energy difference $\varepsilon > 0$ as well as the on-site Coulomb repulsion strengths $U_d > 0$ and $U_p \geq 0$. Second, there are the interatomic hoppings $t_{dp_x} > 0$ along the chains between d and p_x orbitals, $t_{dp_y} > 0$ along the rungs between d and p_y orbitals, and t_{pp} between p_x - p_y orbital pairs. The orbital phases are chosen such that all hopping terms have a constant sign. We use the energy unit $t_{dp_x} = 1$ for numerical results throughout. For superconducting cuprates $t_{dp_x} = t_{dp_y}$ is of the order of 1 eV.

Numerous different values can be found in the literature for these Hamiltonian parameters [2–4, 16–23, 29–31]. Here we are mostly interested in the pairing properties of the Emery ladders presented in Fig. 1 and the pair binding energy (PBE) is the most important observable in our investigation. Therefore, for each ladder structure we have selected a parameter set that yields a significant PBE for two doped holes. The PBE is defined as

$$\begin{aligned}
E_{pb} = & 2E_0(N_\uparrow \pm 1, N_\downarrow) - E_0(N_\uparrow \pm 1, N_\downarrow \pm 1) \\
& - E_0(N_\uparrow, N_\downarrow) \quad (2)
\end{aligned}$$

Ladder	ε	t_{dp_y}	U_d	n_d	E_{pb}
t	2.00	1.1	8	0.69	0.043
g	2.00	1.1	8	0.69	0.027
r	2.00	1.1	8	0.69	0.040
3-chain	2.25	1.1	4	0.72	0.057
5-chain	2.77	1.08	4.62	0.75	0.042
tube	2.25	0.8	4	0.72	0.058

TABLE II. Selected parameters ε , t_{dp_y} , and U_d for the Hamiltonian (1) on each ladder structure. These parameters are used for most results presented here. n_d is the probability of finding a hole in the d orbitals in undoped ladders. E_{pb} is the pair binding energy (2) for two doped holes.

where $E_0(N_\uparrow, N_\downarrow)$ is the ground-state energy of the ladder system with N_σ holes of spin σ . The plus sign is used for hole doping and the minus sign for electron doping. A positive PBE indicates that doped particles (holes or electrons) gain energy by building a bound pair. To find parameters for a given ladder, we start from typical values found in the literature [3] and perform a blind search maximization of the PBE over the free Hamiltonian parameters ε , U_d , U_p , t_{dp_y} , and t_{pp} . Moreover, we require the undoped ladder to be a charge-transfer insulator [32] with the charge ratio of around 3:7 on the p and d orbitals (see Sec. III). When the PBE is positive, we have always found that it is maximal for $U_p = 0$ and $t_{pp} = 0$. The other three parameters are slightly different for each ladder structure, confirming the influence of the oxygen sites. However, to make comparison easier we have selected a single parameter set for the (t,g,r)-ladders. The selected parameters are listed in Table II.

In the noninteracting limit ($U_d = U_p = 0$) one can diagonalize the Hamiltonian (1) exactly for the three common ladder structures in Fig. 1(a) [23]. We have not been able to carry out this calculation analytically for the (t,g,r)-ladders because of their lower symmetries. Nevertheless, one can easily compute their single-particle energy spectrum numerically. We have checked that two single-particle bands cross the Fermi energy in lightly doped ladders with the parameters ε and t_{dp_y} listed in Table II. According to field theory [24] the corresponding interacting system should be a Luther-Emery liquid. In our previous study of the common Emery ladders [23] we found that this generic field-theoretical prediction about two-leg ladders was correct. We can confirm here that this prediction is also correct for the (t,g,r)-ladders, at least for the parameters in Table II.

It is well known that the 2D Emery model and the 2D Hubbard model on a square lattice describe the same low-energy physics for a range of Hamiltonian parameters and band fillings based on the Zhang-Rice mapping [3, 33]. Similarly, one can map the common Emery ladders in Fig. 1 onto a Hubbard ladder, which is known to exhibit pair binding and enhanced pairing correlations [4, 28, 34], although additional hopping or interaction terms are necessary to recover the low-energy physics of hole-doped

Emery ladders [4, 23]. The mapping is more complex for the ladder structures in Fig. 1(b) to (d). In the case of the t-ladder one obtains a two-leg ladder with different parameters on each leg. This asymmetric Hubbard ladder has been investigated recently [35–38]. It also exhibits pair binding and enhanced pairing correlations [38]. The g-ladder and the r-ladder can be mapped onto generalized Hubbard ladders with parameters that alternate from one site to another or from one rung to another, respectively. The pairing properties of such models have not been studied as far as we know.

C. DMRG

For our investigation of the Emery model on two-leg ladders we compute the ground-state properties of the Hamiltonian (1) using the DMRG method [11–15]. This method has been successfully applied to Emery ladders in several studies [4, 16–23]. Our DMRG calculations are carried out using the C++ version of the ITensor Software Library for Tensor Network Calculations [39]. We have validated our program using exact diagonalizations of small clusters [40] and an old DMRG code employed in previous studies [4, 16]. We use bond dimensions up to 9000 resulting in discarded weights of the order of 10^{-8} or smaller. We always start the DMRG calculation with a lower bond dimension and add a noise term (typically 10^{-5}), which is progressively reduced down to zero as the bond dimension increases [41]. We investigate systems with even ladder lengths L up to $L = 40$. To obtain a higher DMRG accuracy, open boundary conditions are used in the leg-direction but we always include oxygen sites at both ladder ends, as illustrated in Fig. 1, because we found that this configuration resulted in weaker boundary effects in our previous work [23]. Nevertheless, finite-size effects may be significant and are discussed when we present our results. In our DMRG calculations the total number of d orbitals is $2L$ while the total number of p orbitals is $4L + 2$ for the (t,g,r)-ladders and the 4-chain tube while it is $3L + 2$ and $5L + 2$ for the 3-chain and 5-chain ladders, respectively.

III. UNDOPED LADDERS

The undoped parent of superconducting cuprates are antiferromagnetic charge-transfer insulators [3, 27, 32]. This state is reproduced by the undoped 2D Emery model for a wide range of parameters. It is also known that the common Emery ladders are charge-transfer insulators with short-range antiferromagnetic order for appropriate parameters [4, 16]. In this section we demonstrate that the (t,g,r)-ladder structures have similar properties for parameters around those listed in Table II.

The gap for charge excitation can be calculated from the ground-state energy E_0 for different number of par-

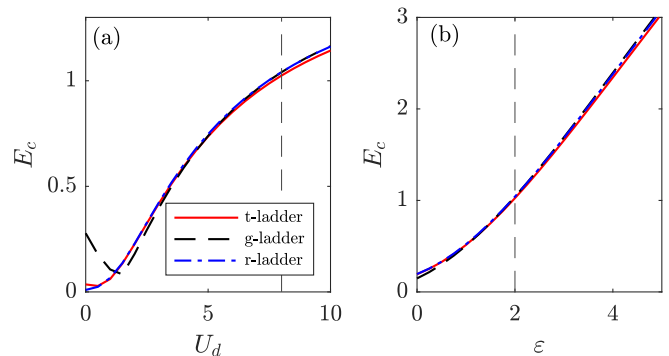


FIG. 2. Charge gaps E_c (3) as a function of the Hamiltonian parameters U_d (left panel) and ϵ (right panel) for undoped (t,g,r)-ladders with length $L = 24$. The other Hamiltonian parameters are given in Table II. Vertical dashed lines indicate the selected values $U_d = 8$ and $\epsilon = 2$, respectively.

ticles using

$$E_c = [E_0(N_\uparrow + 1, N_\downarrow + 1) + E_0(N_\uparrow - 1, N_\downarrow - 1)]/2 - E_0(N_\uparrow, N_\downarrow). \quad (3)$$

In Fig. 2, we show the charge gap as a function of the Hamiltonian parameters U_d and ϵ . Clearly, one can obtain charge gaps of the order of t_{dpx} for reasonable parameter values, as found for the common ladders in previous works [4, 16]. Assuming $t_{dpx} \approx 1$ eV these charge gaps are compatible with experimental values for cuprate ladder materials [42, 43]. Note that the charge gap of the g-ladder does not vanish for $U_d = 0$ in Fig. 2(a). Thus our DMRG result agrees with the single-particle spectrum of the Hamiltonian (1) in the noninteracting limit, which corresponds to a band insulator for this undoped ladder structure. By contrast, the single-particle spectrum of the noninteracting t-ladders and r-ladders is gapless at the Fermi energy corresponding to undoped Emery ladders, in agreement with the vanishing charge gap calculated with DMRG for $U_d = 0$.

The local hole density on orbital i is defined as the the ground-state expectation value of the corresponding hole number operator, $\rho_i = \sum_\sigma \langle n_{i\sigma}^c \rangle$ with $c = d, p$. This density provides us with useful information about the charge distribution in the ground state and the low-energy charge excitations. First, we can define the average densities n_d over all d orbitals and n_p over all p orbitals. In undoped Emery ladders $n_d + \gamma n_p = 1$, where γ is the ratio of p to d orbitals in the unit cell. For the (t,g,r)-ladders and the four-chain tube $\gamma = 2$ but $\gamma = 3/2$ and $5/2$ for the three-chain and five-chain ladders, respectively. Experimentally, the charge ratio on the p and d orbitals is around 3 to 7 for $\text{YBa}_2\text{Cu}_3\text{O}_6$ [26]. We have selected Hamiltonian parameters so that $\gamma n_p/n_d$ reproduces this ratio. The values of n_d are shown in Table II.

The charge gap (3) is calculated by adding two holes or two electrons to the undoped ladders. Thus to understand the nature of low-energy charge excitations we can

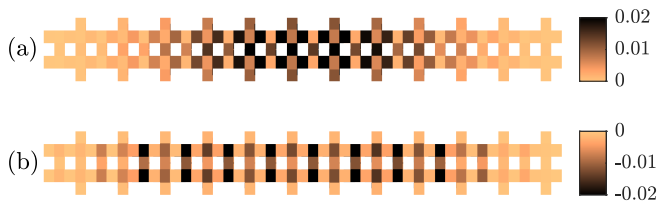


FIG. 3. Normalized hole density variation (5) of the r-ladder with length $L = 24$ and the parameter set in Table II: (a) for two added holes and (b) for two removed holes (= two added electrons) with respect to the undoped ladder.

study the corresponding variation of the local density

$$\Delta\rho_i = \rho'_i - \rho_i \quad (4)$$

where ρ_i is the density of the undoped ladder while ρ'_i designates the density of the ladder with two holes or two electrons added. In Fig. 3 we show the normalized distribution

$$\bar{\rho}_i = \frac{\Delta\rho_i}{\sum_j |\Delta\rho_j|}. \quad (5)$$

for a r-ladder as an example. If the density variation has the same sign for all orbitals i , $\bar{\rho}_i(\delta) = \Delta\rho_i(\delta)/2$. Clearly, added holes primarily occupy p orbitals while holes are mostly removed from d orbitals when electrons are added. Similar results are found for the t-ladders and g-ladders as well as for the common ladders [23]. Therefore, the charge gap, the ground-state charge distribution ratio, and the density variations of low-energy excitations demonstrate that the (t,g,r)-ladders are charge-transfer insulators for parameters around the values given in Table II.

The spin gap can also be calculated from ground-state energies. It is given by

$$E_s = E_0(N_\uparrow + 1, N_\downarrow - 1) - E_0(N_\uparrow, N_\downarrow). \quad (6)$$

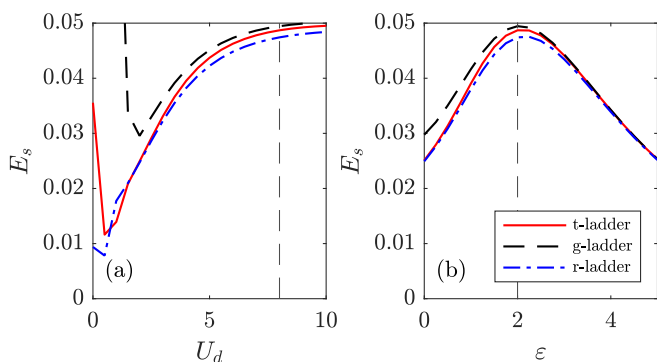


FIG. 4. Spin gaps E_s (6) as a function of the Hamiltonian parameters U_d (left panel) and ϵ (right panel) for undoped (t, g, r)-ladders with a length of $L = 24$. The other Hamiltonian parameters are given in Table II. Vertical dashed lines indicate the selected values $U_d = 8$ and $\epsilon = 2$, respectively.

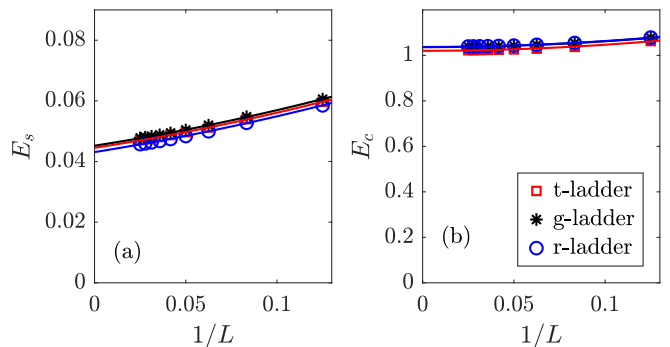


FIG. 5. Convergence analysis of (a) spin gaps E_s and (b) charge gaps E_c as a function of the inverse of the ladder length L in undoped (t,g,r)-ladders with the parameter sets from Table II. Lines represent quadratic fits of the data for $40 \leq L \leq 16$.

Figure 4 shows the spin gap of ladders with length $L = 24$ as a function of the Hamiltonian parameters U_d and ϵ . The spin gaps are clearly much smaller than the charge gaps but these values are comparable to those found in the common ladders [4, 16, 18, 19]. However, the spin gaps are barely larger than the finite-size effects, which can be estimated from the results for $U_d = 0$. As discussed above the single-particle spectra of the t-ladder and the r-ladder are gapless and thus their spin gaps should vanish for $U_d = 0$ in the thermodynamic limit. By contrast, the noninteracting g-ladder has a significantly larger spin gap for small U_d because of the band gap in its single-particle spectrum.

Therefore, we have analyzed the convergence of the spin gaps as a function of the ladder length using DMRG results up to $L = 40$. Some scalings are shown in Fig. 5(a) for the (t, g, r)-ladders with their parameter sets in Table II. Clearly, the spin gaps remain finite in the thermodynamic limit. Moreover, they are compatible with experimental values for cuprate ladder materials [42, 43] assuming $t_{dpx} \approx 1\text{eV}$. Figure 5(b) confirms that finite-size effects are negligible for the corresponding charge gaps in undoped ladders.

Finally, we have verified that the undoped (t,g,r)-ladders have short-range antiferromagnetic order between holes on d orbitals. For this purpose we have calculated the spin-spin correlation function

$$S(r) = \langle S_i^z S_j^z \rangle \quad (7)$$

where $S_i^z = n_{i,\uparrow}^d - n_{i,\downarrow}^d$, i is the index of a d orbital in the middle of the ladder, j designates a d orbital on the same leg, and r is the distance between these two orbitals (in unit of the unit cell of the CuO_2 lattice). In Fig. 6, we show the normalized and staggered correlation functions

$$\hat{S}(r) = \frac{S(r)}{S(r=0)} \cdot (-1)^r \quad (8)$$

for the (t,g,r)-ladders. As expected for spin-gapped two-leg ladders, $\hat{S}(r)$ is positive and decays exponentially

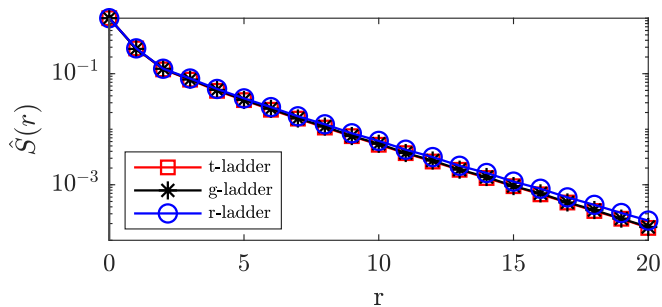


FIG. 6. Spin correlation functions for holes in d -orbitals of undoped CuO_2 ladders-(t,g,r) with length $L = 40$ and the parameter sets from Table II. Lines are guides for the eye.

with the distance r .

In summary, the three ladder structures in Fig. 1(b) to (d) are charge-transfer insulators with short-range antiferromagnetic order for the parameter sets in Table II. Thus the common ladder structures and the novel ones have similar properties when undoped. Although the Hamiltonian parameters have been adjusted, they all lie in a range that is reasonable for superconducting cuprates.

IV. DOPED LADDERS

The Emery model on the common ladder structures exhibits a Luther-Emery phase with PBE and enhanced pairing correlations at low doping in the parameter range that is relevant for the superconducting cuprates [4, 16, 18, 19, 23]. In this section we show that the doped (t,g,r)-ladders can also exhibit this phase.

The evolution of the charge and spin gaps upon doping

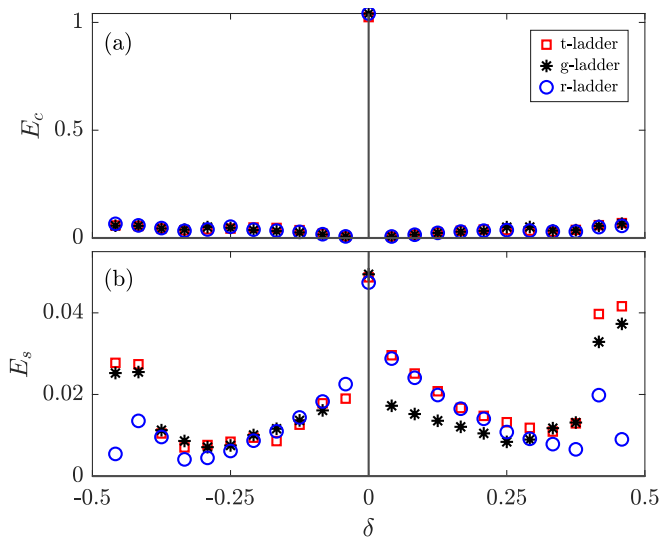


FIG. 7. (a) Charge gap E_c and (b) spin gap E_s as functions of doping δ in (t,g,r)-ladders with a length $L = 24$ and the parameter sets from Table II.

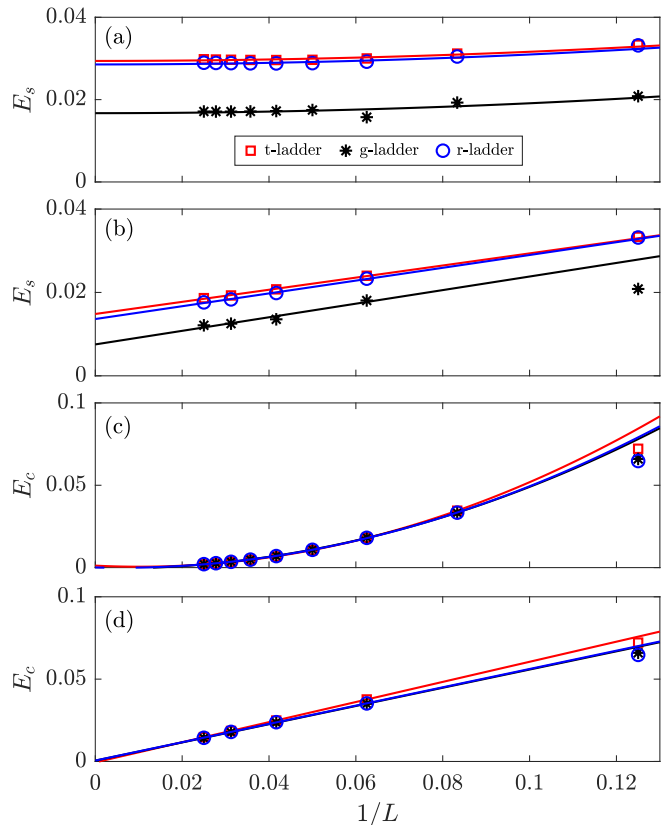


FIG. 8. Convergence analysis of spin and charge gaps as a function of the inverse of the ladder length L in hole-doped (t,g,r)-ladders with the parameter sets in Table II. (a) Spin gaps E_s for two doped holes ($\delta = 1/L$), (b) spin gaps for a fixed doping $\delta = 1/8$, (c) charge gaps E_c for two doped holes ($\delta = 1/L$), and (d) charge gaps for a fixed doping $\delta = 1/8$. Lines represent polynomial fits of the data for $40 \geq L \geq 16$.

is shown in Fig. 7 for the range of $-0.5 < \delta < 0.5$. The charge gap drops from values around $t_{dpx} = 1$ at $\delta = 0$ to much smaller values for $\delta \neq 0$. On the contrary, the spin gaps remain of the same order of magnitude for all dopings shown. This suggests that the doped ladders have gapless charge excitations but only gapped spin excitations as expected for a Luther-Emery phase.

However, the charge and spin gaps shown in Fig. 7 have been calculated in finite ladders of length $L = 24$ and they are again of the order of the finite-size effects for $\delta \neq 0$. As we can only calculate the gaps of ladders up to a length $L = 40$ with our DMRG code, we cannot analyze the finite-size scaling at fixed low doping. Thus we have analyzed finite-size scalings for two doped holes or electrons corresponding to an infinitesimal doping $|\delta| = 1/L \rightarrow 0^+$ in the thermodynamic limit $L \rightarrow \infty$ as well as for a fixed but relatively high doping $|\delta| = 1/8$. Some results are shown in Fig. 8 for each ladder structure with their parameter sets from Table II. Clearly, the spin gaps remain finite in the thermodynamic limit in Fig. 8(a) and (b) while the charge gaps extrapolate to 0 for $1/L \rightarrow 0$ in Fig. 8(c) and (d). Therefore, our re-

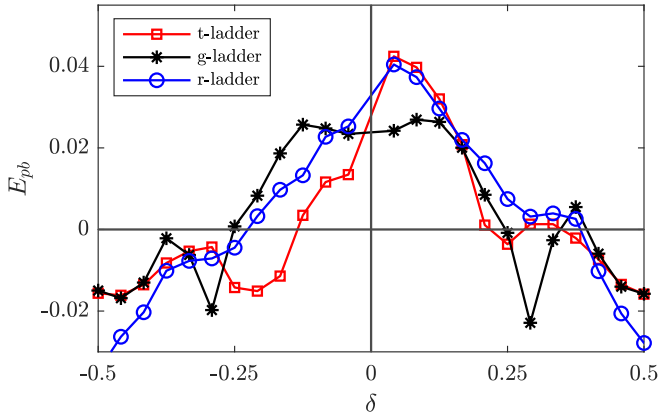


FIG. 9. Pair binding energy E_{pb} as functions of doping δ in doped (t,g,r)-ladders with length $L = 24$ and their respective parameter sets in Table II.

sults indicate a phase, where all spin excitation modes are gapped but (at least) one charge excitation mode is gapless in the thermodynamic limit, which is compatible with a Luther-Emery phase.

The PBE (2) is our primary tool for ascertaining the occurrence of pairing in ladder systems. Figure 9 shows the PBE in the (t,g,r)-ladders for dopings in the range $-0.5 < \delta < 0.5$. In most cases the PBE values are positive at low absolute doping $|\delta|$ but vanish for larger $|\delta|$. Moreover, they are similar in size to the spin gaps, as found for common ladders in previous works [4, 16]. Consequently, these PBE are of the order of the finite-size effects discussed above for the spin gaps. Thus we have also investigated their scaling as a function of the ladder length for two doped particles and at fixed doping $|\delta| = 1/8$. Some scalings are shown in Fig. 10 for the (t,g,r)-ladders with their selected parameters from Table II. Obviously, the PBE converge to small but finite values for $1/L \rightarrow 0$. As we observed for the common ladders [23], the convergence is fast and regular because oxygen sites are included at both ends of all ladder structures, see Fig. 1.

The asymmetry between the PBE for electron and hole doping seen in Fig. 9 is a consequence of our approach. We have searched for Hamiltonian parameters that yield significant positive PBE for hole-doped ladders because we are mostly interested in hole-doped superconducting cuprates. This choice often but not always leads to positive PBE for electron-doped ladders too, as shown by the results in Fig. 9. An obvious remedy would be to select other Hamiltonian parameters based on the PBE for two doped electrons.

Overall the size of the PBE and its evolution in the (t,g,r)-ladders is comparable to the observations made for the common ladders [4, 23]. To support the evidence for pairing provided by the positive PBE, we have computed pairing correlation functions as done in earlier works [16, 18–23]. Here we have focused on the correlations between rung singlet pairs made either of two d

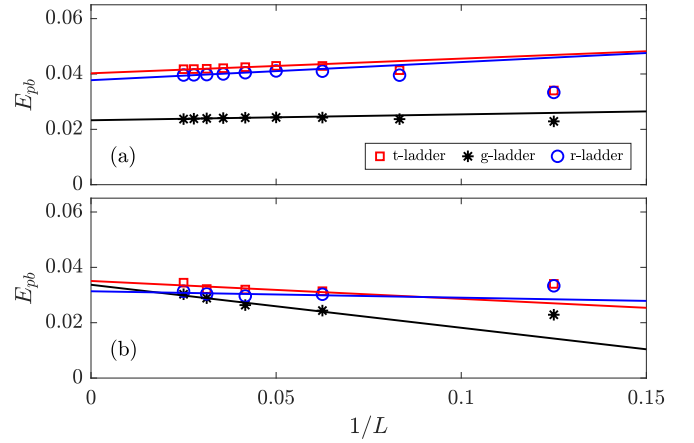


FIG. 10. Convergence analysis of the pair binding energy E_{pb} as a function of the inverse of the ladder length L in hole doped (t,g,r)-ladders with the parameter sets from Table II. (a) For two doped holes ($\delta = 1/L$) and (b) for a fixed doping $\delta = 1/8$. Lines represent linear fits of the data for $40 \geq L \geq 16$.

orbitals or of one d and one p_y orbital because we found previously in the common ladder structures [23] that they were the slowest decaying correlations for electron and hole doping, respectively. Their generic form is

$$P(r) = \frac{1}{2} \left(\langle \Delta_x^\dagger \Delta_{x'} \rangle + \langle \Delta_x \Delta_{x'}^\dagger \rangle \right) \quad (9)$$

where either

$$\Delta_x^\dagger = \frac{1}{2} \left(d_{j\uparrow}^\dagger d_{j'\downarrow}^\dagger - d_{j\downarrow}^\dagger d_{j'\uparrow}^\dagger \right) \quad (10)$$

creates a singlet hole pair in two d orbitals $j = (x, 1)$ and $j' = (x, 2)$ of the same rung x , or

$$\Delta_x^\dagger = \frac{1}{2} \left(d_{j\uparrow}^\dagger p_{yj'\downarrow}^\dagger - d_{j\downarrow}^\dagger p_{yj'\uparrow}^\dagger \right) \quad (11)$$

creates a singlet hole pair in a d orbital $j = (x, 1)$ and the middle p_y orbital of the same rung x . In both cases r is the distance between the rungs x and x' . The expectation value in (9) is calculated for the doped ground state of the Hamiltonian (1).

We have found that pairing correlations $P(r)$ are usually enhanced in the (t,g,r)-ladders when their PBE is positive. Clear results are shown in Fig. 11 for the d - p_y rung correlations (11) in hole-doped ladders with length $L = 40$. The correlation functions are normalized with their value at distance $r = 4$ and shown on a double logarithmic scale as a function of $r - 3$ to avoid large short range oscillations that would skew the analysis of the asymptotic behavior for $r \gg 1$. The correlation functions seem to decay as r^{-1} or slower and thus are clearly enhanced in comparison to noninteracting ladders, where $P(r) \sim r^{-2}$.

The d - d rung correlations (10) are enhanced in the common ladders upon electron doping when the PBE is

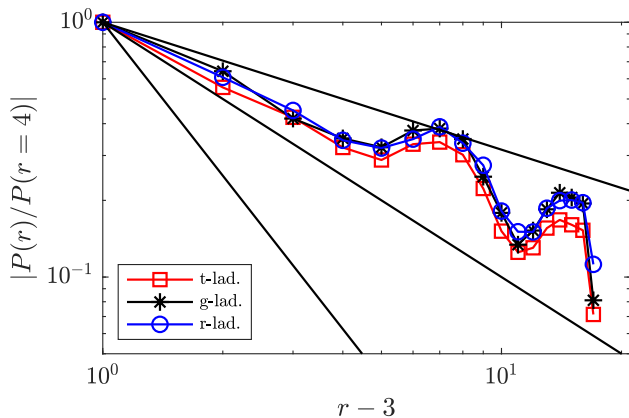


FIG. 11. Pairing correlation functions (9) for singlet pairs on d - p_y rungs (11) in hole-doped (t,g,r)-ladders with length $L = 40$, doping $\delta = 1/8$, and the parameter sets in Table II. Three black lines show a power-law decay $(r-2)^{-\alpha}$ for $\alpha = 1/2, 1$, and 2 .

positive [16, 23]. The picture is less clear for the (t,g,r)-ladder structures discussed here. We have found that the r- and g-ladders usually exhibit enhanced correlations between d - d rung pairs with a r^{-1} decay. These correlations seem to decay faster in the t-ladder but we have renounced drawing a conclusion about a quasi-long-range pairing order due to the limited system size $L \leq 40$ that we can calculate with DMRG. As noted in Sec. II, the t-ladder is related to the asymmetric Hubbard ladder, in which the observed pairing could not be explained by the formation of rung pairs alone [38] due to the absence of the reflection symmetry. Thus it is possible that a quasi-long-range pairing order only becomes clearly visible in electron-doped t-ladders with more complex pair structures than (10) and (11) due to their lower symmetry.

In all Emery ladders that we have investigated, the PBE is not maximal at $t_{dpy} = t_{dpx}$. The four-chain tube is a special case because the periodic boundary condition in the rung direction strongly affects the non-interacting band structure and pairing occurs only for $t_{dpy} < t_{dpx}$ [23]. In the other five ladder structures, allowing $t_{dpy} > t_{dpx}$ leads to larger PBE. However, superconducting cuprates correspond to a 2D Emery model that is invariant under 90 degree rotations and thus to $t_{dpy} = t_{dpx}$. If we want the ladder structures in Fig. 1(b) to (d) to be supercell of the 2D CuO_2 lattice, $t_{dpy} = t_{dpx}$ must be used. Consequently, we have also checked that positive PBE and enhanced pairing correlations occurs in (t,g,r)-ladders with $t_{dpy} = t_{dpx}$. As an example, Fig. 12 compares the doping dependence of the PBE in r-ladders with $t_{dpy} > t_{dpx}$ and with $t_{dpy} = t_{dpx}$ using the same parameters ε and U_d from Table II. Clearly, there is a region with positive PBE at low doping $|\delta|$ in the r-ladder with $t_{dpy} = t_{dpx}$ although this region is narrower than for a r-ladder with $t_{dpy} > t_{dpx}$. Moreover, we see in Fig. 13 that the decay of pairing correlation functions is similar for both sets of parameters.

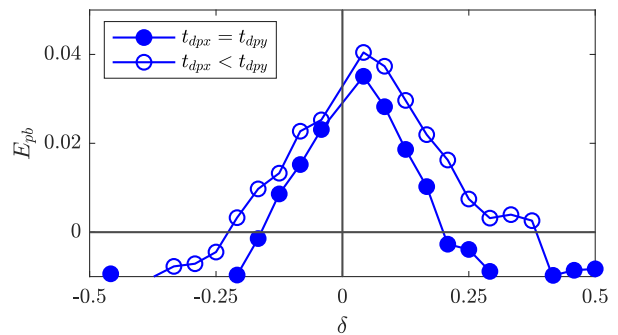


FIG. 12. Pair binding energy E_{pb} as function of doping δ in r-ladders with length $L = 24$. The empty blue circles are the results for the parameter set in Table II, which are already shown in Fig. 9. Solid blue circles show the pair binding energy for the same parameters ε and U_d but $t_{dpx} = t_{dpy}$.

In summary, the (t,g,r)-ladder structures exhibit a Luther-Emery phase with a vanishing charge gap, a positive PBE of the same order as the spin gap, and enhanced pairing correlations. This phase occurs at low doping for a range of parameters that is physically reasonable for superconducting cuprates. The pairing strength and its evolution with doping are similar for the novel and the common ladder structures. For a fixed set of Hamiltonian parameters the pairing strength varies with the ladder structure showing the influence of the oxygen sites. Consequently, one has to select different parameters for each ladder structure to obtain similar values of gaps or PBE. Pairing is also found for $t_{dpy} = t_{dpx}$, although it is weaker than for $t_{dpy} > t_{dpx}$, so that the Luther-Emery phase occurs when the (t,g,r)-ladders can be considered as supercells of the 2D CuO_2 lattice.

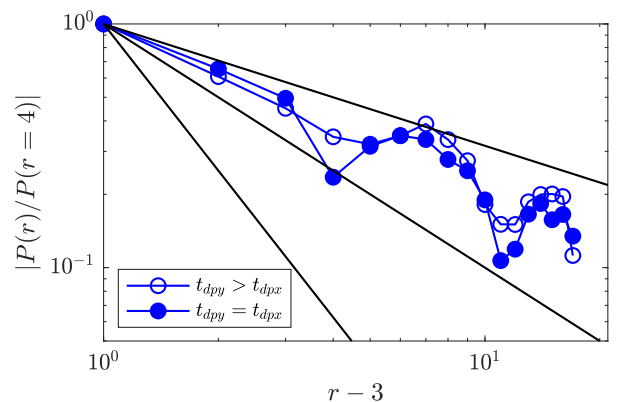


FIG. 13. Pairing correlation functions (9) for singlet pairs on d - p_y rungs (11) in hole-doped r-ladders with length $L = 40$ and doping $\delta = 1/8$. The empty blue circles are the results for the parameter set in Table II, which are already shown in Fig. 11. Solid blue circles show the pairing correlations for the same parameters ε and U_d but $t_{dpx} = t_{dpy}$. Three black lines show a power-law decay $(r-2)^{-\alpha}$ for $\alpha = 1/2, 1$, and 2 .

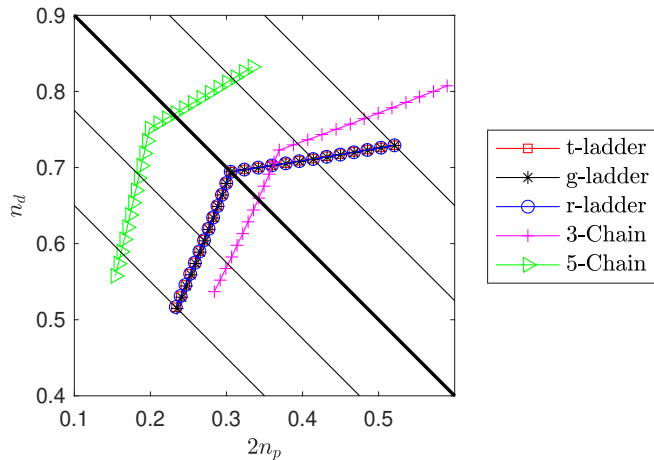


FIG. 14. Relation between the hole occupation n_d of cooper d orbitals and the hole occupation $2n_p$ of oxygen p orbitals on a ladder with length $L = 24$ when the doping δ is varied. Results are shown for the (t,g,r)-ladder structures and two common ladder structures (3-chain and 5-chain) using the parameter sets from Table II. For (t,g,r)-ladders the thick diagonal line corresponds to undoped ladders ($\delta = 0$) while the lower two diagonal lines correspond to constant electron dopings ($\delta = -1/8$ and $-1/4$) and the upper two diagonal lines indicate constant hole dopings ($\delta = +1/8$ and $+1/4$).

V. CHARGE DISTRIBUTION

The question of the charge distribution between Cu and O atoms in the superconducting cuprate layers has attracted a lot of attention recently. Experimental data reveal a correlation between the average occupation n_p of the planar p orbitals of O atoms and the critical temperature for superconductivity when varying the chemical doping or the applied pressure [25, 26]. Several theoretical studies have been carried out to determine the charge distribution between Cu and O orbitals and verify the observed correlation between n_p and the strength of the superconducting state. They include studies of the electronic version of the Emery model on a CuO_2 lattice using cluster methods [5–7] and a study of the hole Hamiltonian (1) on lattices with up to 12×12 sites using a quantum Monte Carlo method [8].

An important issue is the relation between n_p and the average occupation n_d of the planar d orbitals of Cu atoms. In the ladder models considered here they fulfill the sum rule

$$n_d + \gamma n_p = 1 + \delta \quad (12)$$

with the the ratio γ of p to d orbitals (see Sec. III) and the hole doping rate δ . In the superconducting cuprates $\gamma = 2$ and thus recent studies often discuss n_d as a function of $2n_p$ [6–8, 26]. Figure 14 shows the relation between n_d and $2n_p$ in the (t,g,r)-ladder structures with the Hamiltonian parameters from Table II when the doping rate δ is varied. We clearly see that for electron doping most holes are removed from the d orbitals while for

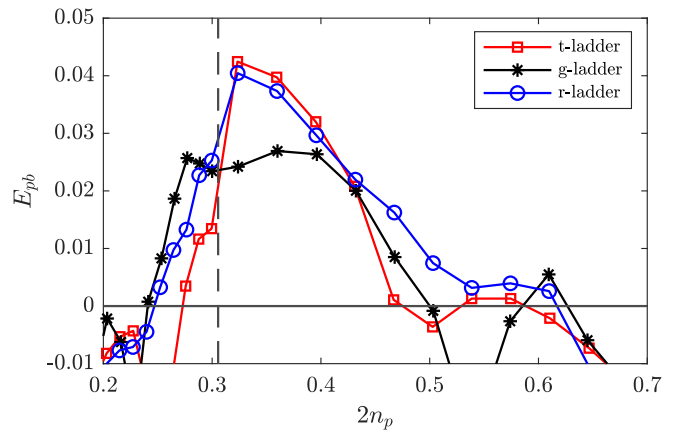


FIG. 15. Relation between the PBE E_{pb} and the oxygen occupation $2n_p$ when the doping δ is varied in (t,g,r)-ladders with $L = 24$ and the parameters from Table II. The vertical dashed line shows $2n_p$ for undoped ladders ($\delta = 0$) with electron doping ($\delta < 0$) on the left-hand side and hole doping on the right-hand side ($\delta > 0$).

hole doping most holes occupy p orbitals, resulting in two lines with different slopes for $\delta < 0$ and $\delta > 0$. This is the behavior expected for a charge-transfer insulator. In the extreme case $t_{dp_x} = t_{dp_y} = 0$ with $U_d > \varepsilon$, one would obtain a vertical line for $\delta < 0$ and a horizontal one for $\delta > 0$. By contrast, a pure Mott-Hubbard insulator yields a straight line (around $\delta = 0$), which becomes vertical in the extreme case $t_{dp_x} = t_{dp_y} = 0$ for $U_d < \varepsilon$. Note that this behavior does not give any evidence about the existence of a Luther-Emery phase. We have indeed verified that the same behavior occurs in the Luttinger liquid phase that is reached when we increase the ratio t_{dp_y}/t_{dp_x} [23].

For comparison, in Fig. 14 we also show the results obtained for the three-chain and five-chain ladders with their respective parameter sets in Table II. First, we note that all results are qualitatively similar with two linear segments, which again just reflects charge-transfer insulators. However, there are clear quantitative differences between the (t,g,r)-ladder structures and the two common ones. In particular, the corners between the two linear segments do not lie on the main diagonal for the three and five-chain ladders although they correspond to undoped ladders. This discrepancy can be easily corrected if we plot n_d as a function of γn_p with $\gamma = 3/2$ and $5/2$, respectively. However, this rescaling also changes the slope of the linear segments and thus impede the analysis of the relations between charge distribution, PBE, and Hamiltonian parameters. Therefore, preserving the ratio of Cu to O atoms is a clear advantage of the (t,g,r)-ladder structures over the common ones when studying these relations.

To illustrate the pairing strength in relation to the charge distribution, Fig. 15 presents a parametric plot of the PBE and the oxygen occupation $2n_p$ when the doping is varied. The same data are shown as E_{pb} versus

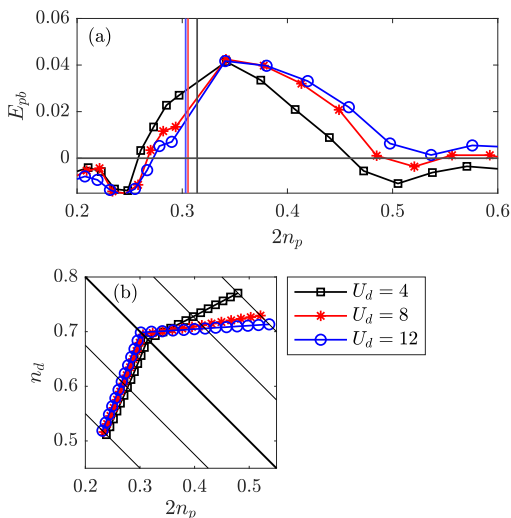


FIG. 16. (a) Relation between the PBE E_{pb} and the oxygen occupation $2n_p$ when doping is varied as in Fig. 15 but for a t-ladder with various interaction strengths U_d . The vertical lines indicate $2n_p$ for undoped ladders. (b) Relation between the copper occupation n_d and the oxygen occupation $2n_p$ as in Fig. 14 but for the same t-ladder as in (a).

δ in Fig. 9. As explained in Sec. II B the undoped ladders correspond to $2n_p \approx 0.3$ due to our choice of Hamiltonian parameters (Table II), in agreement with various superconducting cuprates such as $\text{YBa}_2\text{Cu}_3\text{O}_{6+\delta}$. In Fig. 15 we observe a maximum of the PBE as a function of the oxygen occupation in the range $0.3 \lesssim 2n_p \lesssim 0.4$. This behavior is similar to the parabolic-like dependence of the critical temperature on the oxygen occupation that is found experimentally in superconducting cuprates [25, 26].

Previous studies have shown that the relation between Hamiltonian parameters and pairing strength is quite complex in Emery ladders [4, 16–23]. In contrast, the charge distribution between Cu and O orbitals seems to vary rather systematically. As a first example, Fig. 16(a) presents a parametric plot of the PBE and the oxygen occupation when the doping δ varies for three values of the interaction U_d in a t-ladder. We observe that a larger U_d increases the pairing strength in hole doped ladders but reduces it in electron doped ladders. However, the overall relation between E_{pb} and $2n_p$ is qualitatively similar for the range $4 \leq U_d \leq 12$. In particular, the oxygen occupation of the undoped ladder varies little with U_d in that range, as shown by the vertical lines in Fig. 16(a). Figure 16(b) shows the evolution of the charge distribution between p and d orbitals as δ varies for the same ladders. We see that the slope of n_d versus $2n_p$ is slightly lower for stronger U_d in hole-doped ladders but little change occurs for electron doping. Clearly, doped holes tend to occupy p orbitals to avoid the energy cost U_d of doubly-occupied d orbitals and this trend becomes stronger for higher U_d . In contrast, electrons doping corresponds to removing holes from singly-occupied d orbitals and thus

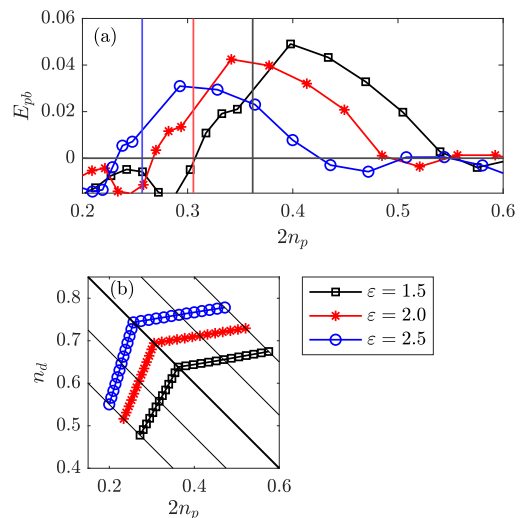


FIG. 17. (a) Parametric plot of the PBE E_{pb} and the oxygen occupation $2n_p$ when doping δ is varied as in Fig. 15 but for a t-ladder with various energy differences ε between oxygen p -orbitals and copper d -orbitals. The vertical lines indicate $2n_p$ for undoped ladders. (b) Copper occupation n_d as a function of oxygen occupation $2n_p$ as in Fig. 14 but for the same t-ladder as in (a).

the relation between n_d and $2n_p$ remains largely unaffected by the value of U_d .

As a second example, Fig. 17(a) presents another parametric plot of the PBE versus the oxygen occupation in a t-ladder but for three values of the energy difference ε between p and d orbitals. We observe an increase of the maximal PBE when ε becomes smaller but the corresponding occupation $2n_p$ of the p orbitals also shifts toward larger values. This shift also occurs in the undoped ladders as shown by vertical lines in Fig. 17(a). Figure 17(b) shows the evolution of the charge distribution between p and d orbitals for the same ladders. As expected, we observe a shift toward a higher occupation of d orbitals when ε is larger. The slope of n_d as a function of $2n_p$ becomes smaller for hole doping but larger for electron doping with increasing ε , and thus tends toward the behavior predicted for a charge-transfer insulator in the limit $U_d > \varepsilon \gg t_{dp_x}, t_{dp_y}$.

We observe a similar dependence of the charge distribution as a function of the Hamiltonian parameters in all three (t,g,r)-ladder structures. (Nevertheless, the pairing strength depends on the structure as illustrated by the PBE values in Table II.) A similar behavior of the charge distribution is observed in 2D Emery clusters [8]. Our results also agree qualitatively with the findings reported for the electronic version of the 2D Emery model [6, 7]. However, when comparing to these results, one has to take into account that varying U_d at fixed ε in our hole Hamiltonian corresponds to varying U_d at fixed $U_d - \Delta$ in the electronic Hamiltonian, where Δ is the energy difference between one electron in a p orbital and one electron in a d orbital. These findings suggest that material-

specific parameters for the Emery model could be determined by comparison with first-principles simulations or experimental data for n_d and n_p [26]. Indeed, the charge distribution of the undoped system determines the energy difference ε between p and d orbitals while the slope of n_d versus $2n_p$ upon hole doping determines the interaction U_d . This comparison is only possible for Emery ladders preserving the Cu to O ratio, such as the ones shown in Fig. 1(b)-(d).

VI. CONCLUSION

Studying strongly-correlated ladder systems is often seen as a way towards understanding their 2D parent systems. In the case of the Emery model for the CuO_2 plane, however, the appropriate choice of ladder structures and model parameters is an issue. For simple models such as the single-orbital Hubbard model on a square lattice, there is an unambiguous two-leg ladder sublattice that is a supercell of the 2D lattice. For the Emery model, however, we can define several different two-leg ladder structures depending on the p orbitals taken into account and the boundary conditions in the rung direction. In our previous paper [23] we showed that the ladder structures used in other works either did not have the right ratio of Cu to O atoms or did not exhibit a Luther-Emery phase for isotropic hoppings.

In this work, we have investigated the Emery model on three ladder-like lattice structures with two legs of copper d -orbitals that are supercell of the CuO_2 plane and thus preserve the ratio of copper to oxygen atoms. For a range of parameters that is physically reasonable for cuprates these ladders describe the same physics as the common ladders studied in previous works despite their lower sym-

metry. They are charge-transfer insulators at a filling of one hole per Cu atom but exhibit a Luther-Emery phase with positive pair binding energy and enhanced pairing correlations at low electron and hole doping. We have explicitly verified that pairing also occurs for isotropic hoppings.

The main advantage of the (t,g,r)-ladder structures is that they can reproduce the distribution of charge between the copper d orbitals and the oxygen p orbitals that is found in the Emery model on the 2D CuO_2 lattice. Thus we can describe the relations between charge distribution, doping, pairing strength, and model parameters in the Luther-Emery phase of doped charge-transfer insulators. Moreover, comparison becomes possible with experimental results for the charge distribution. This is not possible with the common ladder structures due to the incorrect Cu to O ratio or the absence of the Luther-Emery phase for isotropic parameters. Therefore, we think that the ladder structures presented in this work constitute a better approach for studying pairing in the Emery model than the common ladder structures used so far if one aims to investigate the physics of high-temperature superconducting cuprates.

ACKNOWLEDGMENTS

The calculations were carried out on the compute cluster at the Leibniz University of Hannover, which is funded by the Deutsche Forschungsgemeinschaft (DFG, German Research Foundation), project number INST 187/742-1 FUGG.

DATA AVAILABILITY STATEMENT

The data that support the findings of this article are openly available [44].

-
- [1] J. G. Bednorz and K. A. Müller, Possible high T_c superconductivity in the Ba-La-Cu-O system, *Zeitschrift für Physik B Condensed Matter* **64**, 189 (1986).
 - [2] V. J. Emery, Theory of high- T_c superconductivity in oxides, *Phys. Rev. Lett.* **58**, 2794 (1987).
 - [3] E. Dagotto, Correlated electrons in high-temperature superconductors, *Rev. Mod. Phys.* **66**, 763 (1994).
 - [4] E. Jeckelmann, D. J. Scalapino, and S. R. White, Comparison of different ladder models, *Phys. Rev. B* **58**, 9492 (1998).
 - [5] N. Kowalski, S. S. Dash, P. Sémon, D. Sénéchal, and A.-M. Tremblay, Oxygen hole content, charge-transfer gap, covalency, and cuprate superconductivity, *Proceedings of the National Academy of Sciences* **118**, e2106476118 (2021).
 - [6] L.-B. St-Cyr and D. Sénéchal, Effect of the Coulomb repulsion and oxygen level on charge distribution and superconductivity in the Emery model for cuprates superconductors, *SciPost Phys. Core* **8**, 043 (2025).
 - [7] G. L. Reaney, N. Kowalski, A.-M. S. Tremblay, and G. Sordi, Charge gap and charge redistribution among copper and oxygen orbitals in the normal state of the Emery model, *Phys. Rev. B* **112**, 125106 (2025).
 - [8] Y. Peng and M. Jiang, Interplay between Hubbard interaction and charge transfer energy in three-orbital Emery model (2025). *Eprint arXiv:2509.11028*.
 - [9] E. Dagotto, J. Riera, and D. Scalapino, Superconductivity in ladders and coupled planes, *Phys. Rev. B* **45**, 5744 (1992).
 - [10] E. Dagotto and T. M. Rice, Surprises on the way from one- to two-dimensional quantum magnets: The ladder materials, *Science* **271**, 618 (1996).
 - [11] S. R. White, Density matrix formulation for quantum renormalization groups, *Phys. Rev. Lett.* **69**, 2863 (1992).
 - [12] S. R. White, Density-matrix algorithms for quantum renormalization groups, *Phys. Rev. B* **48**, 10345 (1993).
 - [13] U. Schollwöck, The density-matrix renormalization group, *Rev. Mod. Phys.* **77**, 259 (2005).

- [14] E. Jeckelmann, [Density-matrix renormalization group algorithms](#), *Computational Many-Particle Physics*, edited by H. Fehske, R. Schneider, and A. Weiße, volume 739 of Lecture Notes in Physics (Springer, Berlin, 2008), chapter 21, pp. 597–619.
- [15] U. Schollwöck, The density-matrix renormalization group in the age of matrix product states, *Ann. Phys. (NY)* **326**, 96 (2011).
- [16] S. Nishimoto, E. Jeckelmann, and D. J. Scalapino, Differences between hole and electron doping of a two-leg CuO ladder, *Phys. Rev. B* **66**, 245109 (2002).
- [17] S. Nishimoto, E. Jeckelmann, and D. J. Scalapino, Current-current correlations in the three-band model for two-leg CuO ladders: Density-matrix renormalization group study, *Phys. Rev. B* **79**, 205115 (2009).
- [18] J.-P. Song, S. Mazumdar, and R. T. Clay, Absence of Luther-Emery superconducting phase in the three-band model for cuprate ladders, *Phys. Rev. B* **104**, 104504 (2021).
- [19] J.-P. Song, S. Mazumdar, and R. T. Clay, Doping asymmetry in the three-band Hamiltonian for cuprate ladders: Failure of the standard model of superconductivity in cuprates, *Phys. Rev. B* **107**, L241108 (2023).
- [20] H.-C. Jiang, Pair density wave in the doped three-band Hubbard model on two-leg square cylinders, *Phys. Rev. B* **107**, 214504 (2023).
- [21] H.-C. Jiang and T. P. Devereaux, Pair density wave and superconductivity in a kinetically frustrated doped Emery model on a square lattice, *Frontiers in Electronic Materials* **3** (2023).
- [22] L. Yang, T. P. Devereaux, and H.-C. Jiang, Recovery of a Luther-Emery phase in the three-band Hubbard ladder with longer-range hopping, *Phys. Rev. B* **110**, 014511 (2024).
- [23] G. Polat and E. Jeckelmann, Influence of oxygen orbitals and boundary conditions on the pairing behavior in the Emery model for doped ladders, *Phys. Rev. B* **111**, 125137 (2025).
- [24] T. Giamarchi, *Quantum Physics in One Dimension*, International Series of Monographs on Physics (Clarendon Press, Oxford, 2003).
- [25] D. Rybicki, M. Jurkutat, S. Reichardt, C. Kapusta, and J. Haase, Perspective on the phase diagram of cuprate high-temperature superconductors, *Nature Communications* **7**, 11413 (2016).
- [26] M. Jurkutat, C. Kattinger, S. Tsankov, R. Reznicek, A. Erb, and J. Haase, How pressure enhances the critical temperature of superconductivity in $\text{YBa}_2\text{Cu}_3\text{O}_{6+y}$, *Proceedings of the National Academy of Sciences* **120**, e2215458120 (2023).
- [27] D. J. Scalapino, A common thread: The pairing interaction for unconventional superconductors, *Rev. Mod. Phys.* **84**, 1383 (2012).
- [28] R. M. Noack, S. R. White, and D. J. Scalapino, Correlations in a two-chain Hubbard model, *Phys. Rev. Lett.* **73**, 882 (1994).
- [29] M. Ogata and H. Shiba, Holes in two-dimensional CuO_2 system -pairing mechanism emerging from small-cluster studies-, *Journal of the Physical Society of Japan* **57**, 3074 (1988).
- [30] R. L. Martin, Electronic localization in the cuprates, *Phys. Rev. B* **53**, 15501 (1996).
- [31] K. Sheshadri, D. Malterre, A. Fujimori, and A. Chainani, Connecting the one-band and three-band Hubbard models of cuprates via spectroscopy and scattering experiments, *Phys. Rev. B* **107**, 085125 (2023).
- [32] J. Zaanen and A. M. Oleś, Canonical perturbation theory and the two-band model for high- T_c superconductors, *Phys. Rev. B* **37**, 9423 (1988).
- [33] F. C. Zhang and T. M. Rice, Effective Hamiltonian for the superconducting Cu oxides, *Phys. Rev. B* **37**, 3759 (1988).
- [34] R. M. Noack, N. Bulut, D. J. Scalapino, and M. G. Zacher, Enhanced $d_{x^2-y^2}$ pairing correlations in the two-leg Hubbard ladder, *Phys. Rev. B* **56**, 7162 (1997).
- [35] H. Yoshizumi, T. Tohyama, and T. Morinari, Induced Order in Nonequivalent Two-Leg Hubbard Ladder, *Progress of Theoretical Physics* **122**, 943 (2009).
- [36] A. Abdelwahab, E. Jeckelmann, and M. Hohenadler, Ground-state and spectral properties of an asymmetric Hubbard ladder, *Phys. Rev. B* **91**, 155119 (2015).
- [37] A. Abdelwahab and E. Jeckelmann, Correlations and confinement of excitations in an asymmetric Hubbard ladder, *Eur. Phys. J. B* **91**, 207 (2018).
- [38] A. Abdelwahab, G. Polat, and E. Jeckelmann, Pair binding and enhancement of pairing correlations in asymmetric Hubbard ladders, *Phys. Rev. B* **107**, 125117 (2023).
- [39] M. Fishman, S. R. White, and E. M. Stoudenmire, The ITensor Software Library for Tensor Network Calculations, *SciPost Phys. Codebases* **4** (2022).
- [40] A. Weiße and H. Fehske, [Exact diagonalization techniques](#), *Computational Many-Particle Physics*, edited by H. Fehske, R. Schneider, and A. Weiße, volume 739 of Lecture Notes in Physics (Springer, Berlin, 2008), chapter 18–19, pp. 529–577.
- [41] S. R. White, Density matrix renormalization group algorithms with a single center site, *Phys. Rev. B* **72**, 180403 (2005).
- [42] Z. V. Popović, M. J. Konstantinović, V. A. Ivanov, O. P. Khuong, R. Gajić, A. Vietkin, and V. V. Moshchalkov, Optical properties of the spin-ladder compound $\text{Sr}_{14}\text{Cu}_{24}\text{O}_{41}$, *Phys. Rev. B* **62**, 4963 (2000).
- [43] A. Gozar, G. Blumberg, B. S. Dennis, B. S. Shastry, N. Motoyama, H. Eisaki, and S. Uchida, Spin dynamics of $\text{Sr}_{14}\text{Cu}_{24}\text{O}_{41}$ two-leg ladder studied by Raman spectroscopy, *Phys. Rev. Lett.* **87**, 197202 (2001).
- [44] G. Polat and E. Jeckelmann, Pairing and charge distribution in Emery ladders preserving the ratio of Cu to O atoms [data set], LUIS (2026), DOI:10.25835/jdd1qdse.